Network Structure and Properties of Imidazole-Cured Epoxy Novolac Adhesives

PATRICIA A. MADSEN and ROBERT T. FOISTER, *Polymers Department, General Motors Research Laboratories, Warren, Michigan 48090-9055*

Synopsis

The structural characteristics of four epoxy adhesives, obtained by crosslinking an epoxy novolac with various levels of a substituted imidazole curing agent, were investigated and correlated with thermal and mechanical properties. Variations in network structure were characterized by measuring crosslink densities and by qualitatively assessing glassy state free volume from densities and coefficients of thermal expansion. Differential scanning calorimetry was used to obtain glass transition temperatures, and dynamic mechanical thermal analysis was used to follow primary (alpha) and secondary (beta) transitions. Bulk behavior was characterized by tensile modulus, strength, and toughness, together with compressive modulus and yield strength. The effect of sub-T_g aging on compressive yield strength was investigated as well. As the level of imidazole increased, crosslink density, and hence network packing efficiency and free volume, decreased. For fully cured networks, both the glass and the alpha transition temperatures increased with crosslink density. Calculated activation enthalpies and entropies indicated significant degrees of network cooperativity in the alpha transitions, particularly for the more highly crosslinked systems. Beta transition temperatures, however, were found to be independent of crosslink density. Bulk properties generally showed a dependence both on crosslink density and free volume. Yield stress, for example, was highest for the network with lowest crosslink density and free volume. Volume relaxation associated with physical aging also caused yield stress to increase.

INTRODUCTION

Interest in structural adhesive technology, for automotive as well as aerospace applications, has steadily developed over the past decade. This can be attributed in large part to new designs that utilize plastics and composites, which are difficult to join by traditional methods. In addition, adhesives are also being used to replace welding of metallic substrates due to the engineering, cosmetic, and economic advantages they provide. Epoxy-based adhesives, in particular, have been used extensively since they are capable of bonding a variety of substrates, exhibit high cohesive strength, are creep-resistant, and are easily modified by the selection of base resin and hardener, together with polymeric modifiers and fillers.[1]

However, the possible choices for base resins, hardeners, modifying resins, and fillers for epoxy-based structural adhesives are essentially endless, and, in combination, can lead to a variety of adhesives with a myriad of different characteristics. Consequently, for any particular application, mechanical, thermal, and transport properties, viscoelastic response, susceptibility to aging, and durability are all important factors which must be taken into account. Variables that affect these properties include chemical composition,[2-6] cure

Journal of Applied Polymer Science, Vol. 37, 1931–1959 (1989)
 CCC 0021-8995/89/071931-29$04.00

conditions,[7] and thermal history.[8] Changes in these variables cause variations in the network structure of the crosslinked adhesive. Thus, network crosslink density, topology, and free volume are ultimately responsible for the observed material response to factors such as stress, moisture, and thermal cycling. Consequently, it is important to come to a basic understanding of the relationship between network structure and properties for these systems.

Basically, to investigate structure/property relationships in polymeric adhesives, it is necessary to systematically vary composition, cure conditions, or thermal history and then to correlate resultant changes in network structure with changes in properties. Previous work[2-6] in this area has centered on amine cured diglycidyl ether of bisphenol A (DGEBA) epoxies. In this investigation, however, we have focused on networks obtained by crosslinking an epoxy novolac with various levels of a hydroxy-substituted imidazole curing agent. In contrast to amine-cured DGEBA epoxies, imidazole-cured, epoxy novolac adhesives have received relatively little attention.[9,10] We have chosen this class of materials for in-depth investigation as they are the basic components of high strength, durable adhesives recently developed for bonding steel electrodepositied with an organic primer, and sheet molding compound.[11,12]

To answer fundamental questions regarding the relationship between structure and properties in these systems, we have investigated the effect of a systematic variation in imidazole level on the network structure. Furthermore, we have related these changes in network structure to changes in system thermal and mechanical properties. Variations in network structure were characterized by crosslink densities measured in the rubbery state and by differences in relative free volume, assessed by comparing coefficients of thermal expansion and glassy state densities. Network structure was correlated with thermal properties, including glass/rubber and glassy state transitions, low strain mechanical properties, including tensile modulus and compressive modulus and yield strength, and high strain mechanical properties, including tensile strength and toughness. The effect of physical aging[13] on compressive yield stress was also explored.

EXPERIMENTAL

Materials

Material characteristics are summarized in Table I. The epoxy novolac resin, D.E.N. 431, was used as received. The curing agent, 1-(2-hydroxypropyl)-2-methylimidazole, was redistilled (145°C, 2 mm Hg) prior to use. The structure of D.E.N. 431 was provided by the supplier, while the structure of the imidazole was determined by nuclear magnetic resonance (see Fig. 1).

TABLE I
Materials

Material	Supplier	EEW[a]	$\overline{M}_n$	$\overline{M}_w$	$\overline{M}_w/\overline{M}_n$	Comment
D.E.N. 431	Dow Chemical	172–179	400	500	1.25	Epoxy novolac resin
AP-5	Archem Corp.	—	140	—	—	1-[2-Hydroxypropyl]-2-methylimidazole

[a] EEW = epoxy equivalent as provided by supplier.

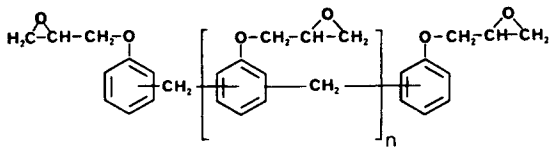

D.E.N. 431; n=0.2

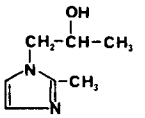

AP-5

Fig. 1. Structures.

Sample Preparation

Four formulations, with ratios of curing agent to epoxide functionality of 0.025, 0.075, 0.113, and 0.150, or 2, 6, 9, and 12 parts per hundred resin (phr) were prepared. These formulations will be referred to as 2 phr, 6 phr, 9 phr, and 12 phr, respectively.

For each formulation the resin was degassed at 100°C for 5–6 h, maintained under vacuum over night, and then reheated to 100°C for 4 h. The mixture was then cooled, and the appropriate amount of curing agent adding under vacuum, after which the mixture was poured into a glass plate assembly to form sheets, or into glass test tubes to form rods. The glass plate assembly consisted of two mold release (Frekote 44) treated, Pyrex glass plates separated by rubber tubing, spaced with stainless steel shims, and held together with binder clips. The test tubes was treated with Frekote Lift release. Following a 24-h gelation at room temperature, each formulation was further cured for 30 min at 150°C in a forced air ove, cooled to room temperature, and demolded. Sheets obtained from this procedure were 3.8 mm and 1.0 mm thick, and rods were 12.7 mm in diameter.

Unless otherwise stated, samples for the experiments described below were cut from the appropriate sheets or rods to the desired geometry using a diamond saw and, when necessary, a TENSILKUT router. All samples were then subjected to a post-cure simulating a typical automotive paint cycle.[1] In addition, since initial evaluations indicated that the post-cure cycle did not completely cure the 2 phr formulation, this system was given further post-cure, as specified below.

[1]Post-cure cycle: 25 min at 200°C, cool to room temperature, 75 min at 160°C, cold water quench to room temperature, 30 min at 135°C, cool to room temperature, 20 min at 135°C, cool to room temperature, 40 min at 160°C, cool to room temperature.

Density and Thermal Expansion Measurements

Room temperature densities were obtained by weighing and measuring the dimensions of specimens (approximately 6.5 × 6.5 × 3.8 mm) cut from a cast sheet. Mass to volume ratios were then calculated.

Thermal expansion data, obtained with 990 Thermal Analyzer coupled with a 943 Thermomechanical Analyzer module (TMA) and Omnitherm Data System, was used to calculate the densities of the sample at T_g + 40°C. Density specimens as described above were heated to a minimum of 40°C above T_g at a rate of 10°C/min. Data were recorded as linear dimension change vs. temperature. The percent dimension change of the specimens from room temperature to $T = T_g$ + 40°C was then obtained. Assuming isotropic expansion, the volume of a specimen at T_g + 40°C was calculated by adding the appropriate percent volume change to the room temperature volume. The high temperature density was then calculated as the ratio of mass to volume at T_g + 40°C.

Measurement of Glass / Rubber and Glassy State Transitions

Differential Scanning Calorimetry (DSC). Glass/rubber transition temperatures (T_g's) of each of the formulations were obtained using a DuPont 1090 Thermal Analyzer with a 912 DSC module. DSC specimens weighing 15–25 mg were cut from 3.8 mm sheets and heated to above T_g at 20°C/min. T_g is reported as the temperature at the transition midpoint, i.e., the temperature at $(1/2)\,\Delta C_p$, where ΔC_p is the change ir heat capacity during the transition.

Dynamic Mechanical Thermal Analysis (DMTA). Dynamic storage moduli and damping ($\tan\delta$) for each of the formulations were measured, as a function of temperature (−150–200°C), at a heating rate of 3°C/min, with a Polymer Laboratories dynamic mechanical thermal analyzer. The multiplexing capabilities of the instrument allowed measurement of material response for five discrete frequencies (0.33, 1.0, 3.0, 10.0, and 30.0 Hz) at a fixed (±2°C) temperature. Rectangular specimens (approximately 20.0 × 12.0 × 1.0 mm) cut from sheets cast in the manner described above were constrained at one end, in single cantilever mode, in a clamping fixture inside an environmental chamber. The primary (or "alpha") glass to rubber transition temperature (T_α) is reported as the maximum in the $\tan\delta$ vs. temperature curve, and the glassy state (or "beta") transition temperature (T_β) is reported as the secondary maximum in the $\tan\delta$ vs. temperature curve.

Stress / Strain Behavior

High Temperature Equilibrium Tensile Modulus. Tensile samples prepared from each of the formulations were tested on an Instron Universal testing machine, Model 1125, with attached environmental chamber and Microcon II data system. Each specimen was allowed to equilibrate in the chamber (maintained at T_g + 40°C) for 30 min prior to testing. Specimens were then strained in small increments, with a strain gage measuring elongation, at a rate of 0.5 mm/min, to a maximum strain of 5%. After each incremental strain the load was allowed to decay to an apparent equilibrium

value. The equilibrium tensile modulus E_e was obtained from a plot of the equilibrium stress vs. strain data. These data were used to characterize the crosslink density of each formulation as described below.

Room Temperature Tensile Modulus and Yield Stress. The tensile modulus of each of the formulations was obtained using an Instron (Model TTC) testing machine. Tensile dogbones were prepared and tested in accordance with ASTM D638. Specimens were pulled, with an extensometer measuring elongation, at a rate of 5 mm/min, to a maximum strain of 10%. Room temperature moduli were determined from the initial slope of the load vs. elongation curve. The maximum stress, or strength at break, and elongation at break were also obtained from these data. Toughness values were calculated from the area under the load vs. elongation curve up to the break point. When possible, yield stress, with yield being defined as the point where stress no longer increases with strain, was also determined.

Room Temperature Compressive Modulus and Yield Stress. The compressive modulus of each of the formulations was obtained using an Instron (Model TTC) testing machine. Compressive rods (12.7 mm in diameter × 25.4 mm in length) were prepared and tested in accordance with ASTM D605. Specimens were compressed at a rate of 5 mm/min, and load measurements were recorded on a strip chart running at 127 mm/min. Room temperature compressive moduli were determined from the initial slope of the load vs. compression curve. Yield stress was also determined from the load vs. compression curve.

In addition, compression samples of each formulation were aged isothermally at temperatures corresponding approximately to T_g − 30°C (133, 120, 110, and 87°C, for 2, 6, 9, and 12 phr, respectively). After 1 week of aging at these temperatures, yield stress was again determined in the manner described above.

For other measured properties, all samples were tested after aging no more than 2 weeks at room temperature. Under these conditions, aging effects (if any) should be very slight, and should not therefore obscure the major trends under investigation.

RESULTS

Physical and Structural Properties

Densities and Coefficients of Thermal Expansion. Densities measured at room temperature increased monotonically with increasing levels of imidazole. The values were 1.198, 1.212, 1.216, and 1.228 g/cm^3 for 2, 6, 9, and 12 phr, respectively. While the coefficients of thermal expansion (CTEs) measured below T_g decreased nonmonotonically with increasing imidazole level, the CTEs measured above T_g increased monotonically. These data are summarized in Table II.

Crosslink Densities (Molecular Weight between Crosslinks). Rubber elasticity theory was used to calculate the average molecular weight between crosslinks (M_c) of the four formulations by means of the following relationship[14]:

$$M_c = \phi\rho RT/G_e \tag{1}$$

TABLE II
Densities (ρ) and Coefficients of Thermal Expansion (CTE)

Formulation	ρ_{RT} (g/cm^3)	CTE ($< T_g$) ($\mu M/M/°C$)	CTE ($> T_g$) ($\mu M/M/°C$)
2 phr	1.198	70.1	147.9
6 phr	1.212	72.9	177.9
9 phr	1.216	71.4	183.2
12 phr	1.228	70.8	185.9

TABLE III
Molecular Weight Between Crosslinks (M_c) and Crosslink Density

Formulation	Test temp[a] (°C)	ρ_T (g/cm^3)	M_c (g/mol)	$1/M_c$ ($\times 10^{-3}$ mol/g)
2 phr	210	1.180	221	4.5
6 phr	200	1.192	334	3.0
9 phr	180	1.199	455	2.2
12 phr	165	1.213	608	1.6

[a] Test temperature approximates T_α (as determined by DMTA at 0.3 Hz) + 40°C.

where ϕ is the front factor, ρ the density at absolute temperature T, R the gas constant, and G_e the equilibrium shear modulus. To apply eq. (1), modulus measurements were made at T_g + 40°C. For small strains, volume is constant during deformation and G_e may be replaced by $E_e/3$, which is one-third the equilibrium tensile modulus.[15] The front factor, ϕ, is the ratio of the mean square end-to-end distance of a network segment to that of a randomly coiled chain, and, following Katz and Tobolsky,[16] is taken to be approximately 1.88.

The density at T_g + 40°C, M_c, and the crosslink density ($1/M_c$) obtained for each of the formulations are listed in Table III. Overall, M_c increased with increasing imidazole level from 221 g/mol for 2 phr to 608 g/mol for 12 phr, or conversely, crosslink density, $1/M_c$, decreased with increasing concentration of the crosslinking agent. As a rough comparison (see the discussion on reaction mechanism below, however), assuming that all epoxy groups react and that the network tie points are ether linkages between reacted epoxy groups, we calculate a theoretical M_c for a completely crosslinked network, with no internal cycles and other defects, of approximately 250 g/mol.

Dynamic Mechanical and Thermal Properties

Dynamic Mechanical Thermal Analysis (DMTA). Most polymers have a characteristic range of dynamic mechanical behavior where the modulus drops by several orders of magnitude as a function of time or frequency, and the material response undergoes a glasslike to rubberlike transition.[17] Ferry[18] has argued that there is a tendency to confuse this behavior with the glass transition which occurs as a function of temperature or pressure, and not time or frequency. When the thermodynamic glass transition is traversed, there is a change in the state of the material with respect to temperature, pressure, and

TABLE IV
Alpha Transition Temperature (°C)

Formulation	Frequency (Hz)				
	0.3	1.0	3.0	10.0	30.0
2 phr[a]	152	156	160	165	168
2 phr[b]	163	168	171	175	178
2 phr[c]	167	170	172	177	179
6 phr	157	161	163	167	169
9 phr	138	141	144	147	151
12 phr	122	127	130	137	139

[a]Standard post-cure.
[b]Additional 3 h at 180°C.
[c]Additional 2 h at 225°C.

internal parameters of order. However, as time or frequency is varied, although material response changes from glasslike to rubberlike, there is no change in the thermodynamic state of the material. To distinguish the temperatures at which these two different phenomena occur, transition temperatures measured as a function of time or frequency are referred to as T_α's, and true glass transition temperatures measured as a function of temperature are referred to as T_g's.

T_α's, reported as the maximum in the tan δ vs. temperature curves, are given in Table IV. Initial runs on standard post-cured samples of the four formulations showed an increase in T_α with increasing frequency, but a nonmonotonic dependence of T_α on imidazole level. There was a maximum in T_α at 6 phr, and this result suggested that the 2 phr was not fully cured.[19] To test this, we post-cured samples of 2 and 6 phr an additional 3 h at 180°C and reran them. The T_α's measured for the 2 phr were as much as 10°C higher than those measured previously, while the T_α's measured for the 6 phr did not change appreciably from the previous runs. Consequently, it was assumed that the 6, 9, and 12 phr samples were essentially completely reacted after the standard post-cure cycle, while the 2 phr required an additional 3 h at 180°C. All samples used in other test methods were subjected to this thermal cycle, unless otherwise stated.

However, subsequent DSC scans (described below) of 2 phr samples revealed that additional curing at an even higher temperature (225°C) had occurred. DMTA runs were again repreated on 2 phr samples that had been subjected to this additional cure. Table IV summarizes the results of these scans, and Figure 2 shows plots of T_α vs. imidazole level for the post curing extremes. Figure 3 illustrates the change in T_α with degree of cure for the 2 phr samples when subjected to different post-cures. Overall, for the post-curing extremes, T_α increased with increasing frequency and decreased with increasing imidazole level.

Using data for the post-cure extremes (standard post-cure cycle + 2 h at 225°C for 2 phr), activation energies for the alpha transition, $E_{A,\alpha}$, calculated from plots of ln frequency vs. $1/T_\alpha$, were 604, 599, 519, and 347 kJ/mol for 2, 6, 9, and 12 phr, respectively. Thus $E_{A,\alpha}$ decreased with decreasing imidazole level (or decreasing crosslink density). In addition, following Starkweather,[20]

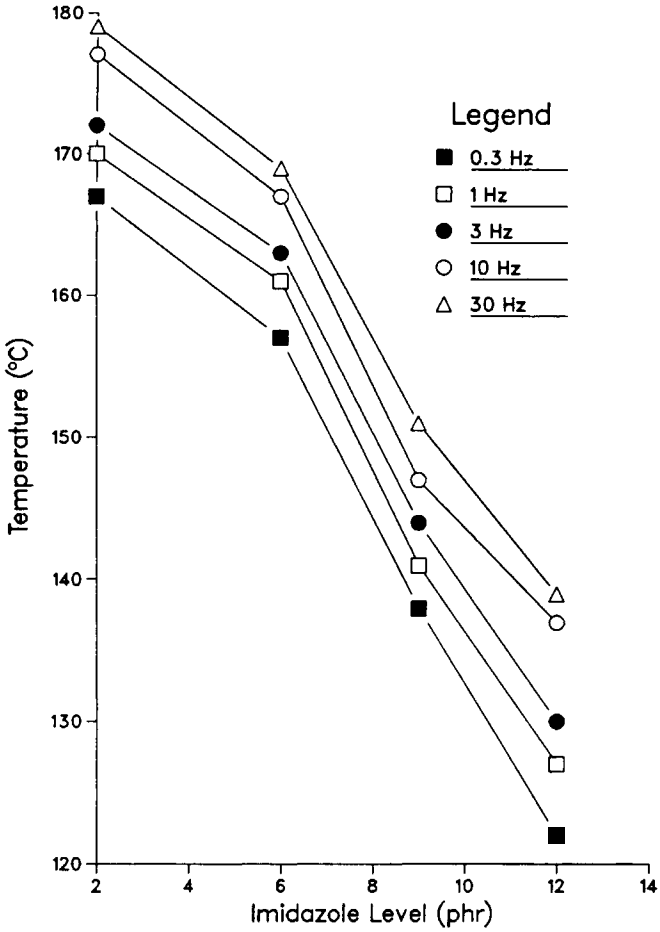

Fig. 2. Alpha transition temperature vs. imidazole level as a function of frequency (Hz): (■) 0.3; (□) 1; (●) 3; (○) 10; (△) 30.

activation entropies for the alpha transition using the earlier measured T_α's and activation energies (again for the post-cure extremes), were calculated from

$$\Delta S_\alpha = (E_{A,\alpha}/T_\alpha) - R[1 + \ln(kT_\alpha/2\pi h)] \quad (2)$$

where T_α is the alpha transition temperature at 1 Hz, k is Boltzmann's constant, h is Planck's constant, and R is the gas constant. The calculated values for the activation entropies are 1120, 1140, 1010, and 628 J/mol K for 2, 6, 9, and 12 phr, respectively.

The heights of the alpha transitions, as measured from the tan δ curves, also exhibited a dependence on crosslink density. As crosslink density decreased, the height of the transition increased, from 0.19 for 2 phr to 0.55 for 12 phr. Alpha transition heights for 6 and 9 phr fell in between at 0.33 and 0.46, respectively. Also, the width of the primary transition was consistently broader for the 2 phr compared to the other systems. Representative curves of

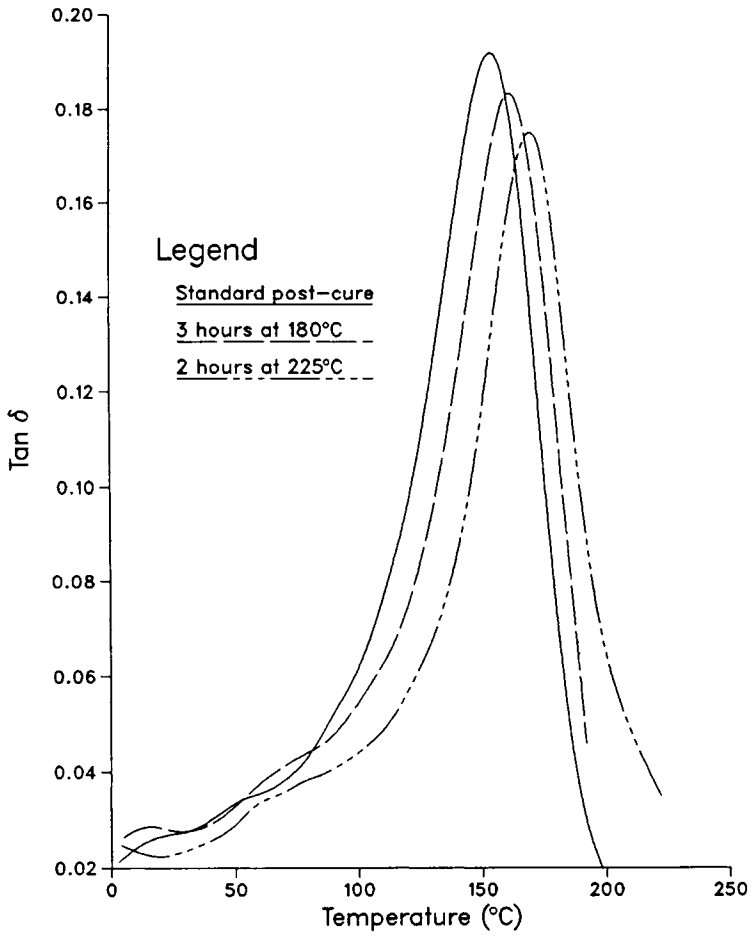

Fig. 3. Alpha transitions (tan δ vs. temperature) as a function of cure time and temperature for 2 phr at 1.0 Hz: (—) standard post-cure; (- - -) 3 h at 180°C; (- —) 2 h at 225°C.

tan δ vs. temperature illustrating these trends at 1 Hz, for the standard post-cure (+3 h at 180°C for 2 phr), are shown in Figure 4. Although additional post curing affected the height of the 2 phr alpha transition, as can be seen in Figure 3, the effect was slight and did not change the overall trend. Also, the heights were found to be essentially independent of frequency. Values for peak height, activation energy, and entropy for the alpha transitions are summarized in Table V.

Glassy state, or "beta", transitions, which correspond to the onset of localized segmental or side group motion,[17] were also apparent for all of the systems. In general, the beta transition temperature (T_β) increased with increasing frequency (Fig. 5) but showed no significant dependence on imidazole level, except for the 2 phr system, which exhibited a very conspicuous shoulder (see Fig. 6). Since there was no dependence of the beta transition temperature on imidazole level, a single activation energy of 81.2 kJ/mol and entropy of 146 kJ/mol K were calculated for the formulations.

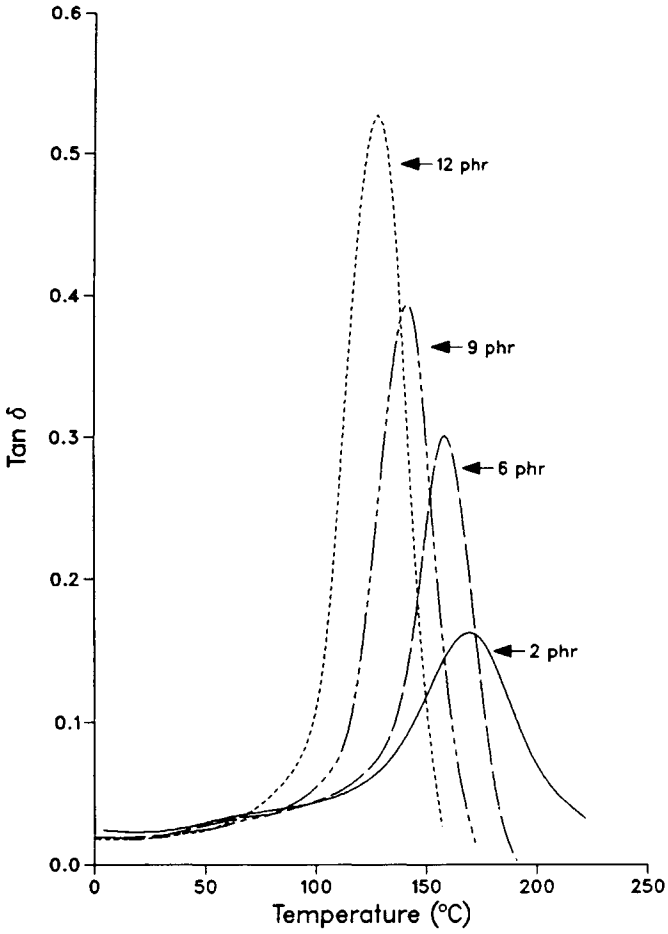

Fig. 4. Alpha transitions (tan δ vs. temperature) for 2, 6, 9, and 12 phr at 1.0 Hz.

TABLE V
Peak Heights, Activation Energies ($E_{A,\alpha}$), and Entropies (ΔS_α) for the Alpha Transition

Formulation	Maximum tan δ[a]	$E_{A,\alpha}$ (kJ/mol)	ΔS_α (J/mol K)
2 phr[b]	0.19	604	1120
6 phr	0.33	559	1140
9 phr	0.46	519	1010
12 phr	0.55	347	628

[a] 0.3 Hz.
[b] Post-cured an additional 2 h at 225°C.

Differential Scanning Calorimetry (DSC). DSC scans for the four formulations subjected to the standard post-cure cycle (+3 h at 180°C for 2 phr) are shown in Figure 7. A maximum in T_g, 161°C, occurred at 6 phr, while T_g's of 160, 143, and 128°C were observed for 2, 9, and 12 phr, respectively. Closer examination of the scans revealed a hint of an exotherm at temperatures greater than 200°C. This suggested that additional curing (or possibly decom-

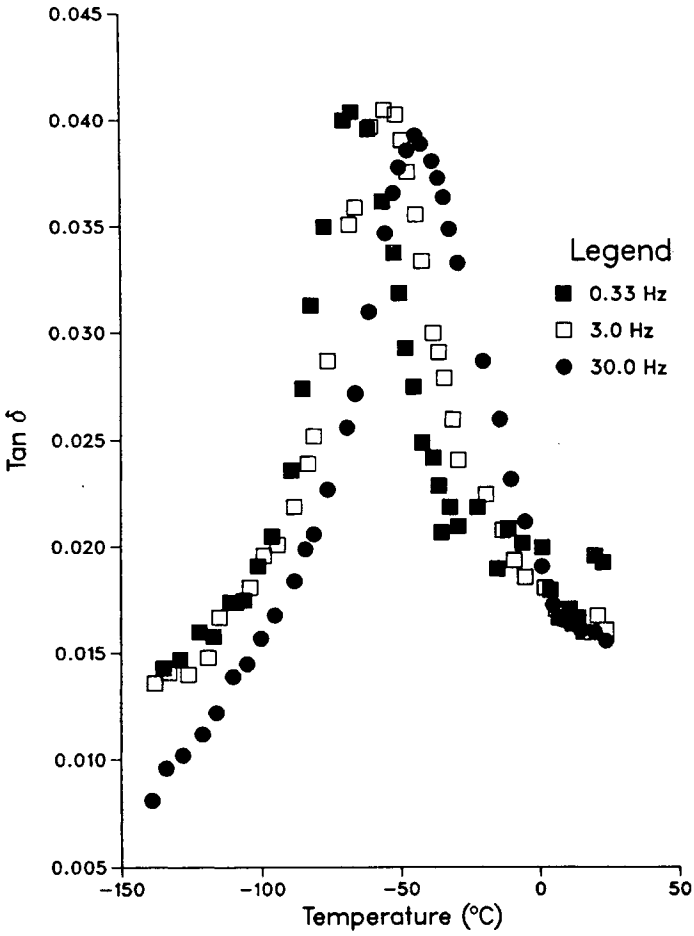

Fig. 5. Beta transitions (tan δ vs. temperature) as a function of frequency (Hz) for 12 phr: (■) 0.33; (□) 3.0; (●) 30.0.

position) was occurring at these temperatures.[21] To test this hypothesis, we repeated the scans after curing the samples an addition 2 h at 225°C. Paralleling the results for the alpha transitions discussed above, this additional post-cure appreciably affected only the 2 phr system, raising its T_g from 160 to 177°C (see Table VI). This second scan is shown as a dotted line in Figure 7. In his work on imidazole curing of epoxies, Vogt[9] found that a minimum of 0.05 mol imidazole/epoxide is necessary to yield a fully reacted system. Below this level, excess epoxy groups always remain unreacted even when the system is extensively post-cured at high (~ 200°C) temperatures. Actually, the 2 phr level corresponds to 0.025 mol catalyst/epoxide. Therefore, it appears that the 2 phr system may not be capable of reaching full conversion, although cure is essentially complete.

Mechanical Properties

Tensile Properties. The room temperature tensile modulus, strength, elongation at break, and toughness values for all the formulations are given in Table VII. As indicated in Figure 8, room temperature tensile modulus

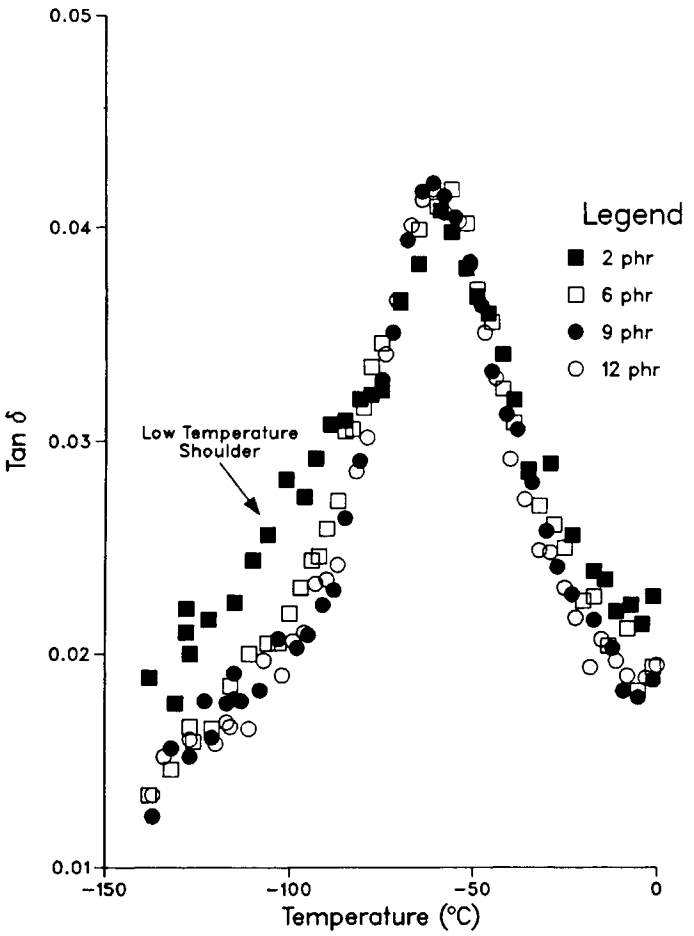

Fig. 6. Beta transitions (tan δ vs. temperature) for 2, 6, 9, and 12 phr at 1.0 Hz: (■) 2 phr; (□) 6 phr; (●) 9 phr; (○) 12 phr.

showed a very slight tendency to decrease with increasing crosslink density.

Strength at break, elongation at break, and tensile toughness all exhibit a minimum at 6 phr, as shown in Figure 9. Except for 2 phr, these properties tended to increase with decreasing crosslink density. As shown in Figure 10, which illustrates typical tensile stress/strain behavior of each system, only the 12 phr sample exhibits well-defined yield at a stress of 9.70×10^4 kPa.

Compressive Properties. Compressive moduli and yield stresses are given in Table VIII. True compressive yield stress (σ_t) was calculated from

$$\sigma_t = P(1 - \epsilon)/A_0 \tag{3}$$

where P is the load at yield, ϵ the strain at yield, and A_0 the initial cross-sectional area of the sample. Equation (3) assumes uniaxial constant volume deformation.[2] As Figure 11 demonstrates, compressive moduli measured at room temperature decreased with increasing crosslink density.

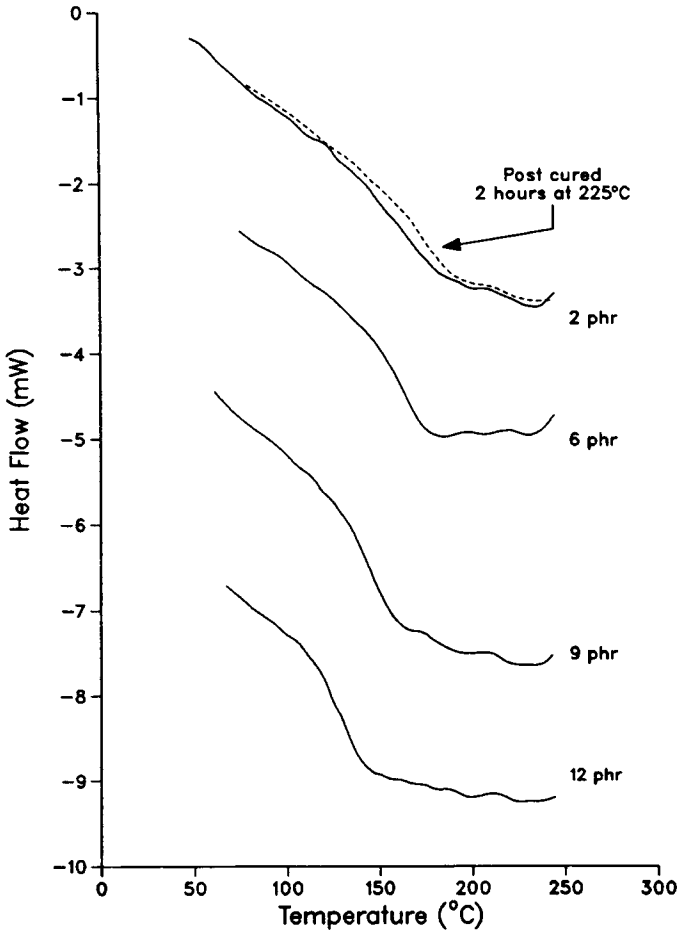

Fig. 7. DSC curves (heat flow vs. temperature) for 2, 6, 9, and 12 phr.

TABLE VI
Glass Transition Temperature (T_g) as Determined by Differential Scanning Calorimetry

Formulation	T_g (°C)	T_g[a] (°C)
2 phr	160	177
6 phr	161	164
9 phr	143	145
12 phr	128	132

[a] Post-cured an additional 2 h at 225°C.

As shown in Figure 12, the yield stress decreased with increasing crosslink density. One week of sub-T_g aging at approximately $T_g - 30$°C caused the measured yield stresses to increase from their unaged values, but the overall trend was unchanged.

TABLE VII
Room Temperature Tensile Properties

Formulation	Modulus ($\times 10^6$ kPa)	Strength ($\times 10^4$ kPa)	Elongation at break (%)	Toughness (J)
2 phr	3.05 ± 0.09	7.19 ± 0.44	3.4 ± 0.4	1.9 ± 0.4
6 phr	3.08 ± 0.17	6.32 ± 0.43	2.8 ± 0.3	1.2 ± 0.3
9 phr	2.94 ± 0.27	6.97 ± 1.51	3.1 ± 0.3	1.8 ± 1.1
12 phr	3.14 ± 0.14	0.70 ± 0.04	6.4 ± 0.8	6.0 ± 0.8

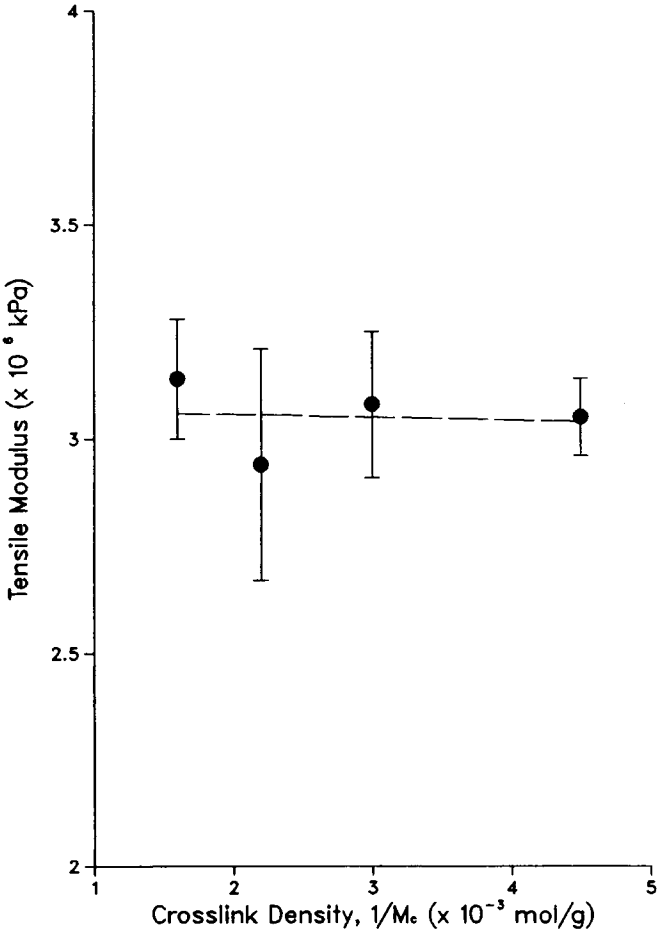

Fig. 8. Tensile modulus vs. crosslink density.

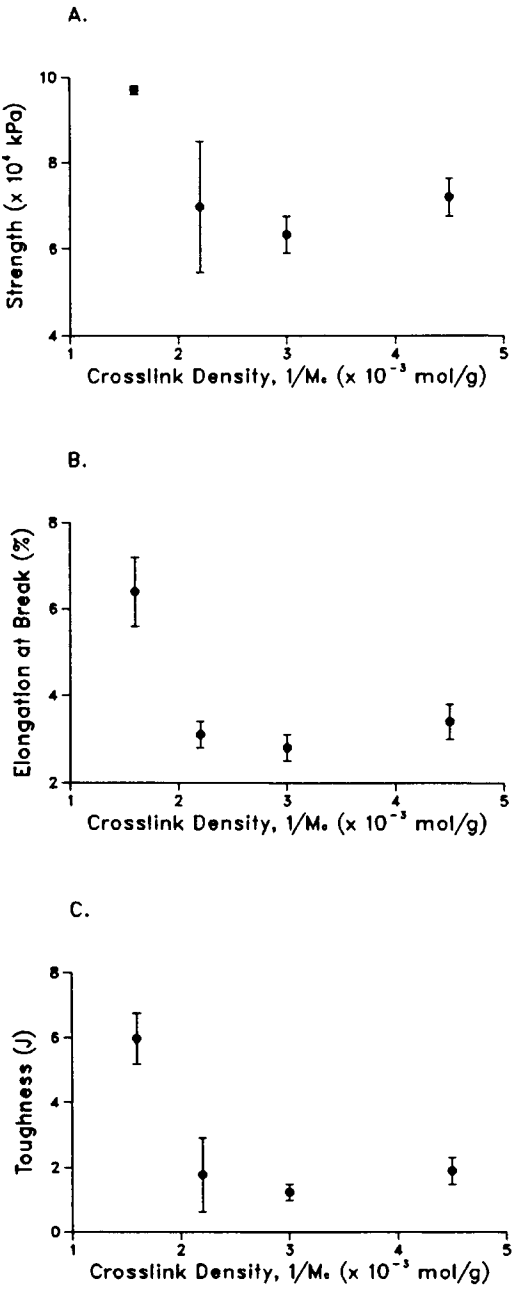

Fig. 9. Tensile strength (A), tensile elongation at break (B), and tensile toughness (C) vs. crosslink density.

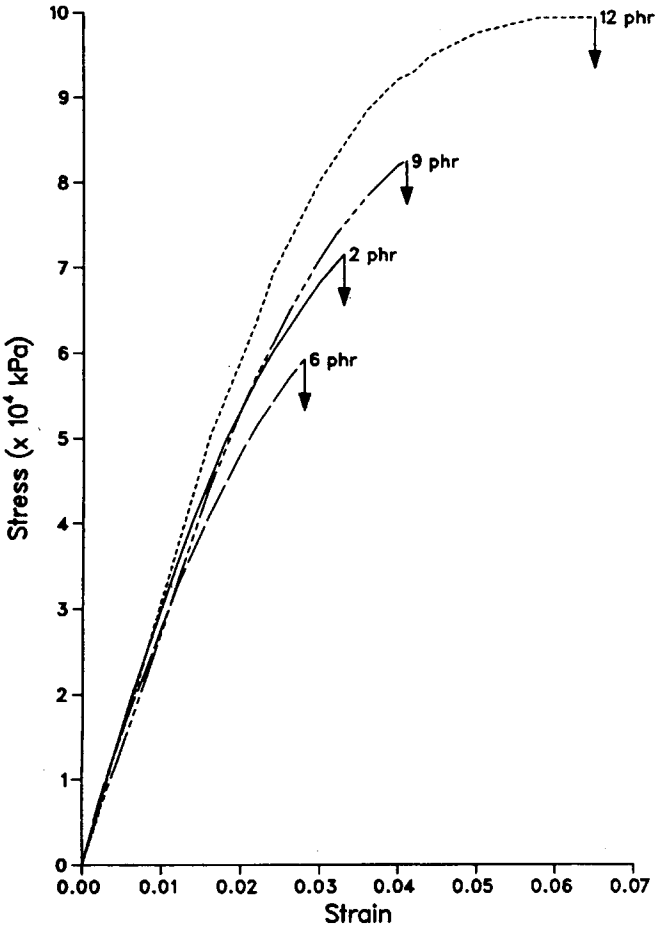

Fig. 10. Tensile stress/strain behavior.

TABLE VIII
Compressive Modulus and Yield Stress (σ_t)

Formulation	Modulus ($\times 10^6$ kPa)	σ_t ($\times 10^5$ kPa)	$\sigma_{t\ age}$[a] ($\times 10^5$ kPa)
2 phr	2.32 ± 0.06	1.25 ± 0.01	1.27 ± 0.05 (133°C)
6 phr	2.33 ± 0.04	1.29 ± 0.02	1.33 ± 0.02 (120°C)
9 phr	2.43 ± 0.07	1.33 ± 0.01	1.39 ± 0.01 (110°C)
12 phr	2.58 ± 0.04	1.34 ± 0.02	1.41 ± 0.02 (87°C)

[a]Aged 1 week at indicated temperature.

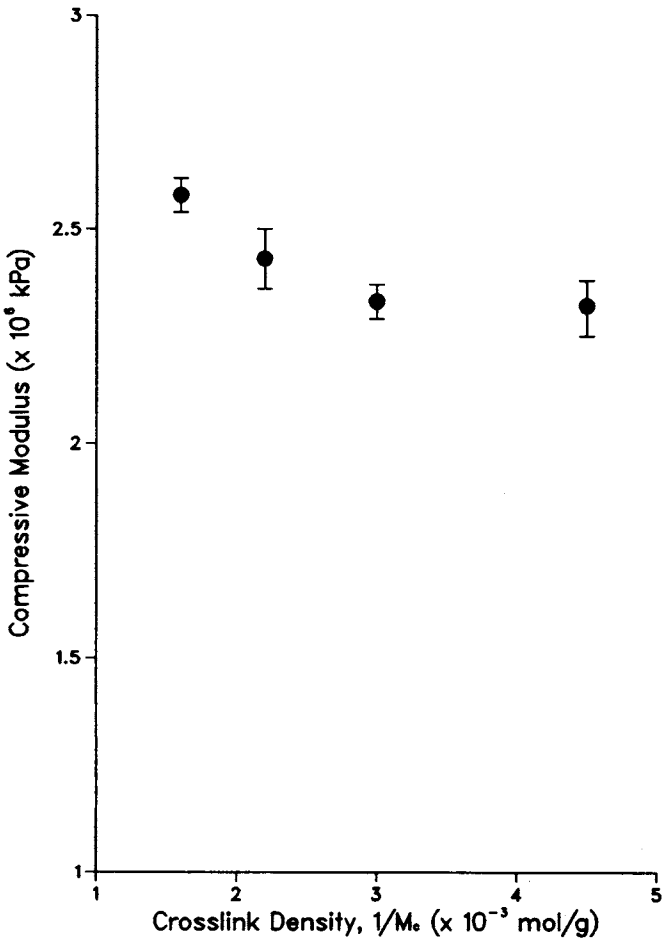

Fig. 11. Compressive modulus vs. crosslink density.

Summary of Results

For convenience, and for use in conjunction with the discussion that follows, results and general trends are summarized in Table IX.

DISCUSSION

Network Formation

Although detailed kinetic studies of the crosslinking reaction mechanism were not undertaken in this work, it is reasonable to regard the hydroxy-substituted imidazole as the primary catalytic species. In studies of model reactions of various imidazoles with monofunctional (i.e., noncrosslinking) phenyl glycidyl ether, Ricciardi et al.[10] have established at least two pathways whereby, in principle, imidazole may be regenerated (hence act as a true catalyst) during the course of polymerization. In our case, however, since earlier work[22] revealed no evidence of regenerated imidazole, we have assumed

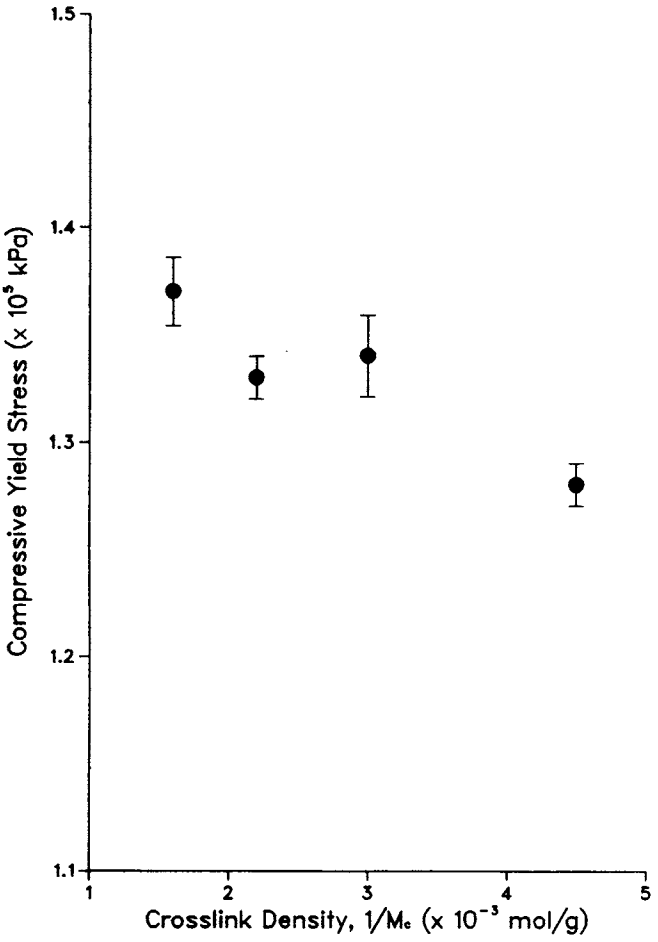

Fig. 12. Compressive yield stress vs. crosslink density.

that the imidazole is largely incorporated into the crosslinked polymer network.

Crosslink Density, Molecular Weight Between Crosslinks, and Network Topology. If the imidazole is incorporated into the polymer network, one possible pathway is via a "Lewis Base" mechanism.[23] The primary crosslink points would then be ether linkages. Intuitively, and as demonstrated by Berger and Lohse[24] in their work using 1-MIA and phenyl glycidyl ether monomer, one would expect the degree of polymerization, and therefore the degree of crosslinking, to increase with increasing imidazole level. However, as noted above, we observed the opposite trend. One possible explanation for this is the probability of side reactions. In particular, Dusek[25] has reported that side reactions are especially prevalent when the reaction mechanism is homopolymerization, which is equivalent to catalytic polymerization, the likely mechanism for reaction of the imidazole and epoxy.

Two possible side reactions which would tend to increase M_c are internal cyclization and chain transfer. In recent reviews on network formation in curing of epoxy resins, Dusek,[25] Oleinik,[26] and Rozenberg,[27] all discuss inter-

TABLE IX
Summary of General Trends

Property	Variation with increasing	
	Imidazole level	Crosslink density
T_α	Decreases	Increases
T_g	Decreases	Increases
T_β	No effect	No effect
$(\tan \delta)_{max}$	Increases	Decreases
$E_{\alpha,\alpha}$	Decreases	Increases
ΔS_α	Decreases	Increases
Density (ρ)	Increases	Decreases
Tensile modulus	Increases[a]	Decreases[a]
Tensile strength	Increases	Decreases
Tensile elongation at break	Increases	Decreases
Tensile toughness	Increases	Decreases
Compressive modulus	Increases	Decreases
Compressive yield strength (σ_t)	Increases	Decreases

[a] Weak dependence.

nal cyclization, or the formation of elastically inactive cycles in epoxy networks. It is reasonable to expect that as more imidazole is incorporated into the network the probability of internal cyclization (involving for hydroxyl[26] as well as epoxy groups) increases. Such loops would be elastically inactive, and therefore would not contribute to the measured rubbery modulus, from which crosslink density is calculated.

Just as an increase in the degree of polymerization can lead to an increase in the probability of cycle formation, it can also lead to an increase in the probability that chain transfer reactions occur.[26] Rozenberg[27] describes chain transfer to alcohol or other proton-donor compounds as the most common process among the chain termination reactions in the catalytic polymerization of epoxies. Since the imidazole curing agent is substituted with a hydroxyl group, as more catalyst is available for polymerization, more hydroxyl groups are also available for chain transfer with the alkoxide ions generated from epoxy groups during the polyetherification reaction. This chain transfer would effectively terminate growing network chains. Consequently, there would be less groups available for crosslinking, resulting in a decrease in crosslink density with an increase in imidazole level.

Free Volume. Below the glass transition occupied volume increases uniformly with temperature while the equilibrium free volume remains approximately constant.[28] This amount of free volume is too small to allow the large chain conformations associated with the glass/rubber transition to occur. Above T_g, however, free volume increases with temperature, as expressed by the following linear relationship:

$$f = f_g + \alpha_f(T - T_g) \tag{4}$$

where f is the fractional free volume, V_f/V, f_g is the fractional free volume at T_g, and α_f is the coefficient of expansion of the free volume, which is approximately equal to the difference in expansion coefficients above and below T_g.[17] This expression gives a quantitative description of the variation of free volume with temperature. From the CTE data given in Table II, it is readily apparent that α_f increases significantly as the crosslink density decreases. For 2 phr, which has the highest crosslink density, the difference in CTE above and below T_g is 77.8 $\mu M/M/°C$, while for 12 phr, which has the lowest crosslink density, the difference is almost 50% higher, at 115 $\mu M/M/°C$.

Since the amount of free volume in a polymer network is a function of the packing of the molecular segments, density (or specific volume) is a measure of this packing. As detailed above, densities measured at room temperature (Table II) increased monotonically with decreasing crosslink density. Thus, the network with the highest crosslink density also has the highest specific volume. This type of implied relationship between crosslink density and free volume has been reported previously.[3,5,9]

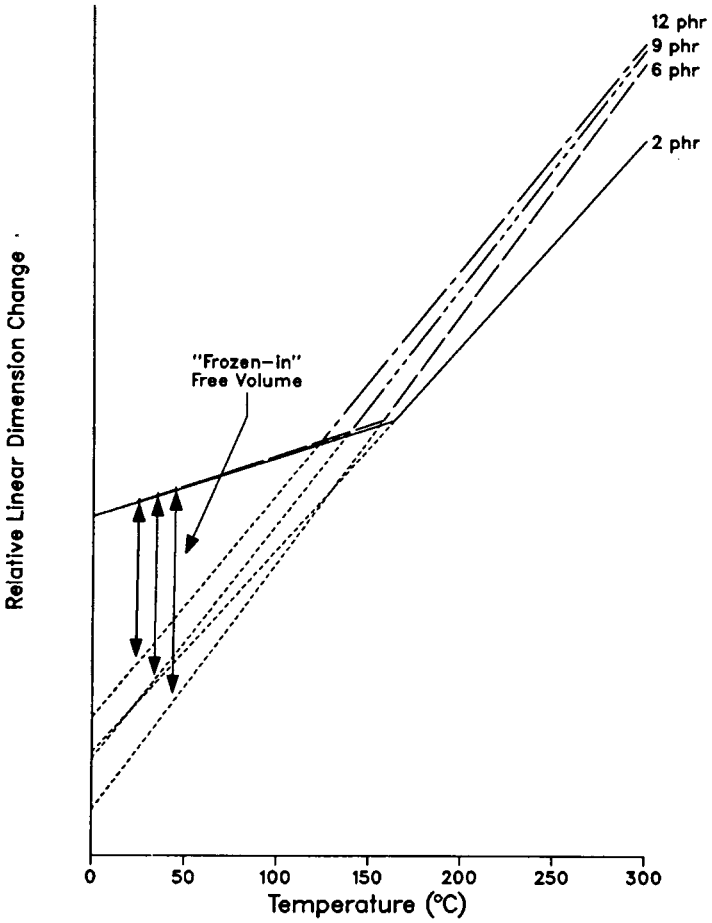

Fig. 13. Linear dimension change vs. temperature for 2, 6, 9, and 12 phr.

The relationship between crosslink density and free volume can also be illustrated using the CTE data given in Table II. Figure 13 shows a plot of relative linear dimension change vs. temperature for each of the formulations. The dotted lines are the extrapolated equilibrium lines. Theoretically, this is proportional, for isotropic materials, to the volume the networks would occupy if they were cooled at an infinitesimally slow rate. Below T_g, the difference between the CTE curve and the extrapolated equilibrium curve is indicative of the nonequilibrium free volume frozen into the network due to cooling at a finite rate. Generally, as can be inferred from Figure 13, the free volume at room temperature increases with crosslink density.

Thermal and Dynamic Mechanical Properties

The degree of crosslinking and the amount of associated free volume affect both the glass and alpha transitions since the creation of network junctions can alter chain mobility. Whether the degree of crosslinking and the amount of free volume affect the beta transition depends on the degree of network cooperativity involved in the associated molecular motion. Consequently, their effect on the beta transition may not be universal.[7,26] In the systems investigated here, the glass and alpha transitions were found to depend on crosslink density, while the beta relaxations were found to be independent.

The Glass Transition. For systems which had been fully cured, T_g was found to decrease with crosslink density. Nielson[28] found that, for a number of different polymers, T_g varied linearly with crosslink density. However, as is apparent in Figure 14, a plot of T_g vs. crosslink density was not linear. However, if the data point for the 2 phr system is ignored, a slope of 1.2×10^4 g °C/mol for 6, 9, and 12 phr is obtained, which is comparable to the slope obtained by Nielson, 3.9×10^4 g °C/mol. The fact that the 2 phr system has a glass transition temperature less than that predicted by the general trend for the other three systems is undoubtedly related to the fact that this system has not reached full conversion, and would not necessarily follow the trend for the fully reacted systems with higher imidazole concentrations.

The Alpha Transition. Figure 4 indicates that at a constant frequency there is a systematic decrease in T_α with crosslink density. Additionally, the damping heights were found to decrease with increasing crosslink density, while the activation energies of the alpha transitions were found to increase with crosslink density (Table V). The decrease in peak height with increasing crosslink density implies that the number of molecular segments involved in the transition was reduced, and the increase in T_α with crosslink density indicates that the activation energy for motion of molecular segments has increased.[7] The increase in T_α and activation energy, and the decrease in peak height for the alpha transition with an increase in crosslink density is, like the variation in T_g with crosslink density discussed above, due to a reduction in molecular mobility as network crosslink density increases. Also noteworthy, as shown in Figure 4, is the relative broadness of the alpha peak for the 2 phr system. Interestingly, Gupta et al.[3] have attributed this type of broadness to an imperfect network caused by unreacted epoxy molecules. This is consistent with the discussion above, where it was pointed out that the 2 phr network has not reached full conversion.

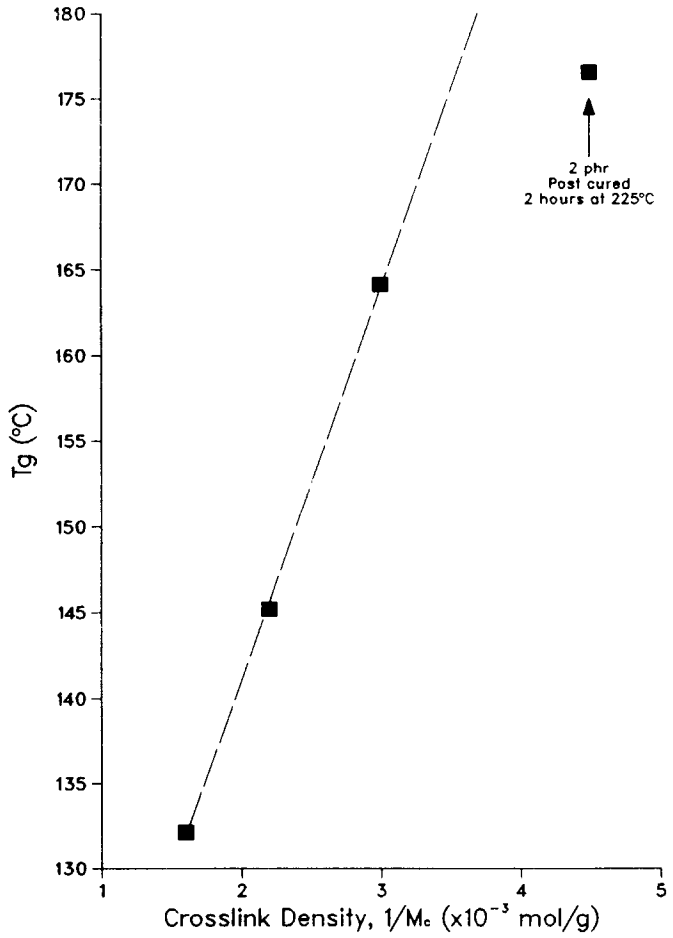

Fig. 14. Glass transition temperature vs. crosslink density: (■) 2 phr, post-cured, 2 h at 225°C.

The Beta Transition. Figure 6 demonstrates that there is no significant change in the peak temperature or magnitude of the beta transition with decreasing crosslink density. The widths of the transitions were also essentially constant with increasing crosslink density, except for 2 phr, which had a very conspicuous shoulder on the low temperature side. Similar to the width of the alpha transition discussed above, this shoulder has been attributed to the motion of unreacted epoxy groups.[4,26]

Since, for a given frequency, there were no obvious differences in beta transition temperatures, an average activation energy of 81.2 kJ/mol was calculated. This constant activation energy indicated that the local motion responsible for the beta transition is not significantly influenced by variations in network structure. There have been reports that network structure has little or no effect on the beta transition.[26] In contrast, other work suggests that the beta transition depends on crosslink density.[7] However, these investigations all involved different methods, resins, and curing agents. As was stated above the dependence of the beta transition on network structure is in all

probability a function of the particular group(s) involved in the motion as well as the degree of network cooperativity required.

Mechanical Properties

Mechanical properties can be generally divided into high and low strain categories. Overall, we found that the high strain properties (tensile strength, elongation, and toughness) exhibited a dependence on crosslink density, while low strain properties (tensile and compressive modulus, compressive yield stress) varied with the amount of glassy state free volume.

Tensile Modulus. Moduli measured in the glassy state have been reported to be both dependent and independent of crosslink density. For example, Chang et al.[7] have found, for a series of networks formed from the diglycidyl ether of butanediol cured with 4,4′-diaminophenyl sulfone, that the tensile modulus increased with crosslink density. On the other hand, Yamini and Young[2] have found, for a series of epoxy resins cured with triethylenetetramine, that the tensile modulus decreased with increasing crosslink density. Nielson,[28] however, has reported that the glassy state moduli of a series of chemically similar networks with different crosslink densities exhibited no dependence on crosslink density, while Vogt[9] reports a nonmonotonic dependence on crosslink density for various imidazole-cured epoxy networks.

In spite of these qualitatively different trends, it is generally agreed that intermolecular forces are the predominant factors in determining modulus in the glassy state.[3,7,26] Crosslink density does not appear to play a direct role since the intermolecular forces in the glassy state dominate and suppress the effects of intramolecular forces, at least at low strains.[26] However, free volume at the test temperature should play a role. For example, we have argued that the network with the highest crosslink density (2 phr) also has the highest free volume. Consequently, since molecular mobility in this network is comparatively high, it should require less force to achieve a given strain, which means that it should have the lowest modulus at room temperature. It could be argued that this trend is apparent in the data in Figure 8. However, the tensile modulus for these systems appears to depend only weakly on network structure in the glassy state. As discussed below, the compressive moduli more clearly reflect differences in free volume.

Tensile Strength, Elongation at Break, and Toughness. As noted above (see also Table VII), tensile strength, elongation at break, and toughness (measured as the area under the stress/strain curve) all exhibit a minimum at 6 phr. However, if we ignore the data for 2 phr, the trend is for these properties to increase with decreasing crosslink density. Again, the fact that the data for 2 phr do not follow the trend for the fully reacted systems is probably related to the fact that the system has not reached full conversion.

Ultimate tensile strength, elongation at break, and toughness, as opposed to tensile modulus, are high strain properties, and are therefore expected to depend on crosslink density. Intuitively, one might expect tensile strength to increase with the crosslink density because covalent bonds, such as those involved in crosslinks, must be broken to initiate fracture. In actuality, however, high degrees of crosslinking can render the network sensitive to the presence of flaws.[28]

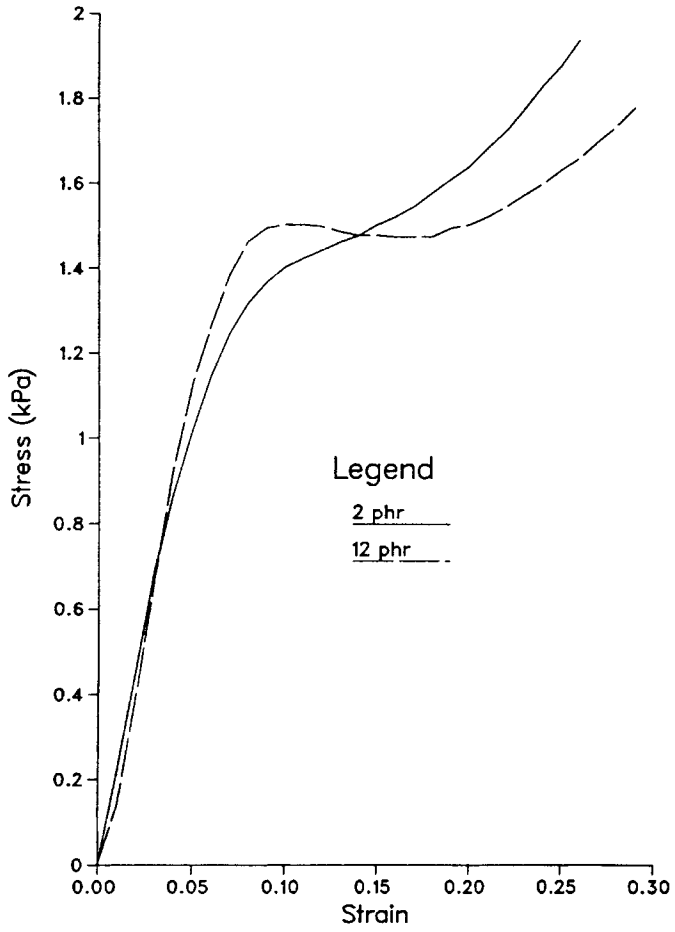

Fig. 15. Compressive stress/strain behavior: (—) 2 phr; (- - -) 12 phr.

It is apparent from the stress/strain behavior illustrated in Figure 10 that the 2, 6, and 9 phr specimens failed with very little detectable plastic deformation. This type of behavior is indicative of brittle fracture, where the stress/strain curve is almost linear up to fracture and the strain at fracture is low, of the order of a few percent.[29] The 12 phr samples did show some evidence of plasticity prior to failure.

Behavior of the Systems in Compression. As shown in Figures 11 and 12, the room temperature elastic modulus and the yield stress measured in uniaxial compression decreased with increasing crosslink density. This behavior is consistent with an increase in free volume for the more highly crosslinked systems. As discussed above, the network with the higher density and lower free volume will generally exhibit a higher modulus, since more stress would be required to deform the network. Likewise, as free volume decreases and the molecules become more tightly packed, more force is required to initiate yielding and associated plastic flow.

Evident in Figure 15, which illustrates the compressive stress/strain behavior of 2 and 12 phr, is the absence in the 2 phr curve of "strain softening," or a

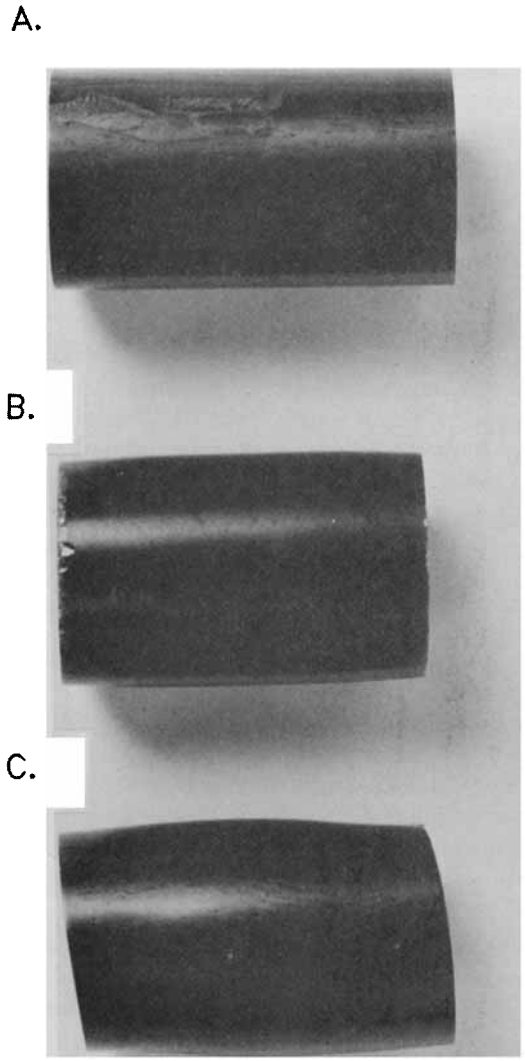

Fig. 16. Undeformed (A), 2 phr at yield (B), and 12 phr at yield (C), compression samples.

post-yield decrease in stress with increasing strain. Microscopically, strain softening is a process that causes a structural change to take place after yielding which then allows flow to occur and continue at lower stresses.[30] Only the 12 phr samples exhibited true strain softening. It is likely that the more highly crosslinked networks are not able to maintain flow after the onset of yield due to rapid orientation hardening. All the networks, however, eventually did exhibit hardening at higher strains. It should also be noted that generally the yield point was less pronounced in the more highly crosslinked systems.

Macroscopically, there were very significant differences in the compressive behavior of the highest and lowest crosslink density systems. Figure 16 shows an untested compression sample, a 2 phr sample at yield, and a 12 phr sample

at yield. As is evident in the photograph, while the 2 phr sample bulges slightly at yield, the 12 phr sample also exhibits shear offset of the top half with respect to the bottom half of the sample, suggesting that considerable shear deformation or flow has occurred. This type of deformation results from the formation of shear bands, which can only form if the material is strain softening. These shear bands show as birefringence,[30] and their existence in fracture surfaces of the 12 phr samples was confirmed with optical micrographs. No such birefringence patterns were observed for the 2 phr samples.

Finally, scanning electron micrographs of the compressive fracture surfaces indicated a change in failure mode with crosslink density. Figure 17 shows the failure surface of a 2 phr sample. Cleavage stops (brittle failure bands) and chips, typical of brittle failure, are clearly evident. Cleavage stops are formed where there are inhomogeneities (e.g., impurities and voids) in the material. At the inhomogeneity, the fracture front divides into several sections which reunite as the fracture progresses. In this way, steplike patterns are produced, as well as chips that splinter off.[31] The failure surface of a 12 phr sample is also shown in Figure 17. Cleavage stops are also evident in this micrograph. In addition, however, the presence of drawn out fibrils indicates that possibly some plastic deformation may have occurred prior to failure.[31]

Effect of Physical Aging

As amorphous solids are cooled at finite rates through the glass/rubber transition, they do not reach immediate thermodynamic equilibrium at temperatures below T_g.[13] Volume, enthalpy, and entropy relaxation studies of glassy polymers have demonstrated that these systems undergo slow processes which attempt to establish equilibrium. This gradual approach to equilibrium affects many material properties and is termed "physical aging."[13]

The effect of aging on compressive yield stress was specifically investigated for the systems of different crosslink density. Since the rate of aging is a function of the difference between the aging temperature and the glass transition temperature, each formulation was aged 1 week at a temperature of approximately $T_g - 30°C$. Under these conditions, as summarized in Table VIII, the yield stress at room temperature for a given system generally increased. This is due to the densification process which occurs during aging, resulting in a more tightly packed network with less free volume. The data in Table VIII also indicated that the magnitude of the aging effect was greatest for the system of lowest crosslink density.

CONCLUDING REMARKS

The network structure, thermal behavior, and mechanical properties of four epoxy networks, prepared by crosslinking a novolac resin with a substituted imidazole, were found to vary with the amount of crosslinking agent used. The decrease in T_g with increasing imidazole level was explained in terms of increased probability of side reactions (internal cyclization and chain transfer) and chain end groups, all of which lower the number of functional groups available for crosslinking and create elastically inactive chains. For fully cured networks, T_g increased with crosslink density. Primary dynamic mechanical, or alpha, transition temperatures were also found to increase with increasing

A.

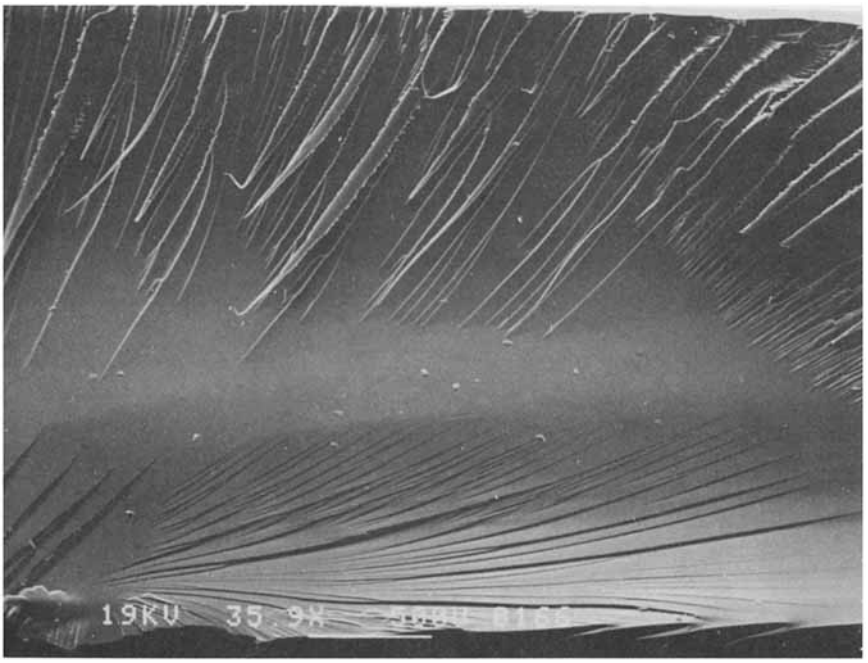

B.

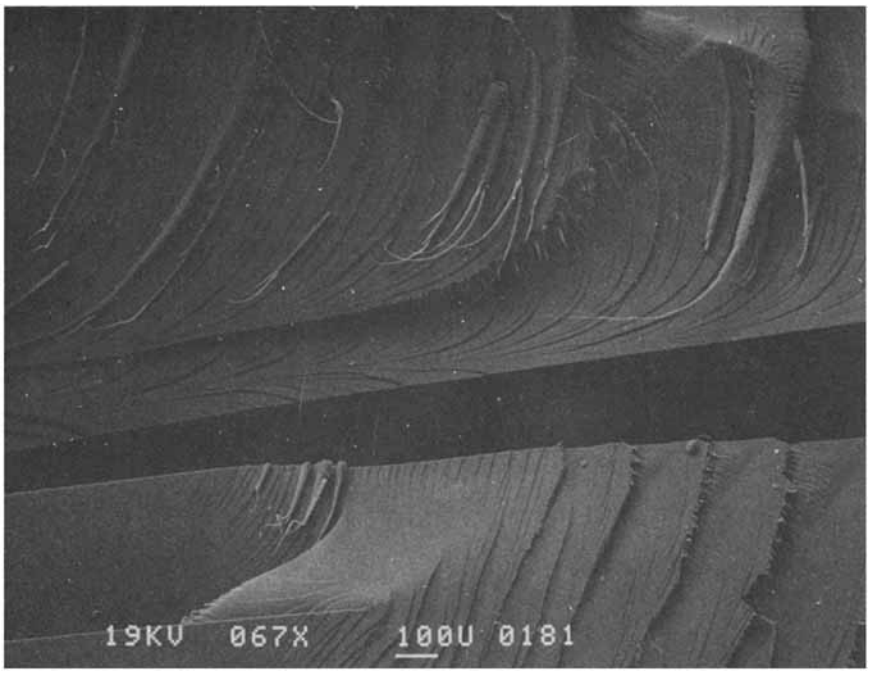

Fig. 17. Scanning electron micrographs of 2 phr (A) and 12 phr (B), compression sample failure surfaces.

crosslink density, while the beta transitions exhibited no dependence on crosslink density. The amount of glassy state free volume frozen into the networks was also found to depend on crosslink density. It was inferred that the more highly crosslinked systems contained more free volume due to packing constraints imposed by crosslinks.

Low strain mechanical properties, including tensile and compressive modulus and compressive yield strength, increased with decreasing crosslink density. Due to more efficient molecular packing in the glassy state, the less crosslinked networks required more force to achieve a given network strain. Also, sub-T_g aging increased the yield strength more for lower than for the higher crosslinked systems. Measured high strain mechanical properties, including tensile strength, elongation at break, and toughness, tended to increase with decreasing crosslink density. It was argued that a less tightly crosslinked network can better distribute applied loads through segmental mobility and, therefore, tolerate higher stresses and strains before failing.

Overall, it has been demonstrated that systematic changes in imidazole level can have a pronounced effect on the structural, thermal, and mechanical properties of crosslinked epoxy novolac networks. A subsequent publication will deal with the relationship between structure and viscoelastic response in these same systems.

The authors are grateful to Dr. T. S. Ellis for his comments concerning the DSC measurements and to Dr. J. A. Schroeder for the optical micrographs and several helpful discussions.

References

1. J. Shields, *Adhesives Handbook*, 3rd ed., Butterworths, London, 1984.
2. S. Yamini and R. J. Young, *J. Mater. Sci.*, **15**, 1814 (1980).
3. V. B. Gupta, L. T. Drzal, G. Y-C. Lee, and M. J. Rich, *Polym. Eng. Sci.*, **25**(13), 812 (1985).
4. V. B. Gupta, L. T. Drzal, C. Y-C. Lee, and M. J. Rich, *J. Macromol. Sci. Phys.*, **B23**(4–6), 435 (1984–85).
5. R. J. Morgan, F-M. Kong, and C. M. Walkup, *Polymer*, **25**, 375 (1984).
6. J. D. Lemay, B. J. Swetlin, and F. N. Kelley, in *Characteristics of Highly Crosslinked Polymers*, S. S. Labana and R. A. Dickie, Eds., American Chemical Society, Washington, DC, 1984.
7. T. D. Chang, S. H. Carr, and J. O. Britain, *Polym. Eng. Sci.*, **22**(18), 1213 (1982).
8. V. B. Gupta and L. T. Drzal, *J. Appl. Polym. Sci.*, **30**, 4467 (1985).
9. J. Vogt, *J. Adhesion*, **22**, 139 (1987).
10. F. Ricciardi, W. A. Romanchick, and M. M. Joullie, *J. Polym. Sci., Polym. Chem. Ed.*, **21**, 1475 (1983).
11. R. T. Foister and R. K. Gray, U.S. Pat. 4,544,432, 1985.
12. T. J. Dearlove and R. K. Gray, U.S. Pat. 4,383,060, 1981.
13. L. C. E. Struik, *Physical Aging in .. orphous Polymers and Other Materials*, Elsevier, Amsterdam, 1978.
14. L. R. G. Treloar, *The Physics of Rubber Elasticity*, Clarendon, Oxford, 1958.
15. H-G. Elias, *Macromolecules*, Vol. 1, Plenum, New York, 1977.
16. D. Katz and A. V. Tobolsky, *Polymer*, **4**, 417 (1963).
17. I. M. Ward, *Mechanical Properties of Solid Polymers*, Wiley-Interscience, London, 1971.
18. J. D. Ferry, *Viscoelastic Properties of Polymers*, 3rd ed., Wiley, New York, 1980.
19. *EPON Resin Structural Reference Manual*, Shell Oil Company.
20. H. W. Starkweather, *Macromolecules*, **14**, 1277 (1981).
21. R. B. Prime, in *Thermal Characterization of Polymeric Materials*, E. A. Turi, Ed., Academic, New York, 1981.
22. J. A. Schroeder, P. A. Madsen, and R. T. Foister, *Polymer*, **28**, 929 (1987).

23. H. Lee and K. Neville, *Handbook of Epoxy Resins*, McGraw-Hill, New York, 1967, p. 5–4.
24. J. Berger and F. Lohse, *Polym. Bull.*, **12**, 535 (1984).
25. K. Dusek, in *Advances in Polymer Science 78*, K. Dusek, Ed., Springer-Verlag, Berlin/Heidelberg, 1986.
26. E. F. Oleinik, in *Advances in Polymer Science 80*, K. Dusek, Ed., Springer-Verlag, Berlin/Heidelberg, 1986.
27. B. A. Rozenberg, in *Advances in Polymer Science 75*, K. Dusek, Ed., Springer-Verlag, Berlin/Heidelberg, 1986.
28. L. E. Nielson, *J. Macromol. Sci., Rev. Macromol. Chem.*, **C3**(1), 69 (1969).
29. E.H. Andrews, *Fracture in Polymers*, Elsevier, New York, 1968.
30. P. Bowden, in *The Physics of Glassy Polymers*, R. N. Haward, Ed., Wiley, New York, 1973, Chap. 5.
31. L. Engel, H. Klingele, G. W. Ehrenstein, and H. Schaper, *An Atlas of Polymer Damage*, Prentice-Hall, Englewood Cliffs, NJ, 1981.

Received December 8, 1987
Accepted April 20, 1988